CHAPTER 20

# The Mercator Ocean Global High-Resolution Monitoring and Forecasting System

Jean-Michel Lellouche[1], Eric Greiner[2], Olivier Le Galloudec[1], Charly Régnier[1], Mounir Benkiran[1], Charles-Emmanuel Testut[1], Romain Bourdallé-Badie[1], Marie Drévillon[1], Gilles Garric[1], and Yann Drillet[1]

*[1]Mercator Océan, Ramonville Saint Agne, France; [2]CLS, Ramonville Saint Agne, France*

*Mercator Ocean monitoring and forecasting systems are routinely operated in real time since early 2001. They have been regularly upgraded through several systems of increasing complexity, expanding the geographical coverage from regional to global, improving models and assimilation schemes. In this chapter we give a description of the current Mercator Ocean real-time, global high-resolution system. The ocean model, the observations, and the data assimilation scheme are detailed with a particular focus to the specifics of the Mercator Ocean system. Technical details about the real-time operation of the system are given. The system is then examined through a scientific evaluation, highlighting the level of performance and the reliability of the system. User needs and evolutions of the system are finally drawn.*

## Introduction

Over the past 20 years, the use of data assimilation methods for operational ocean forecasting systems has been extensively developed. A number of operational systems have emerged at the national and international scale within the international GODAE (Global Ocean Data Assimilation Experiment) project, and then within the GODAE OceanView (Schiller et al., chapter 2 of this book). Mercator Ocean is the French contribution to this initiative that aims to describe and forecast changing ocean conditions by running predictive models that work on a principle used successfully by meteorological models to forecast atmospheric conditions.

Mercator Ocean monitoring and forecasting systems have been routinely operated in real-time in Toulouse since early 2001 and regularly upgraded through four prototypes of increasing complexity (PSY1, PSY2, PSY3, and PSY4). These upgrades expanded the geographical coverage from regional to global and improved models and assimilation schemes (Brasseur et al., 2006; Lellouche et al., 2013). After having successfully coordinated the European MyOcean and MyOcean2 projects (http://www.myocean.eu), Mercator Ocean was officially entrusted by the European Commission on November 11, 2014 to implement and operate the Copernicus Marine Environment Monitoring Service (CMEMS), as part of the European Earth observation program

Lellouche, J.-M.., et al., 2018: The Mercator Ocean global high-resolution monitoring and forecasting system. In "*New Frontiers in Operational Oceanography*", E. Chassignet, A. Pascual, J. Tintoré, and J. Verron, Eds., GODAE OceanView, 563-592, doi:10.17125/gov2018.ch20.

Copernicus (http://marine.copernicus.eu). Mercator Ocean opened the CMEMS in May 2015 and is in charge of the global high resolution ocean analyses and forecasts. Since then, research and development activities have been conducted to improve the real-time 1/12° high-resolution (eddy-resolving) global analysis and forecasting system. The main ingredients of an analysis and forecasting system are 1) an ocean numerical model, 2) available observations in the past, and 3) data assimilation techniques based on mathematical methods. The goal of a data assimilation method is to force the ocean model to be as close as possible to the observations available in the past in order to obtain the best forecasts in the future, taking into account observations and model errors, as illustrated in Fig. 20.1. Since October 19, 2016, Mercator Ocean has delivered real-time daily services (weekly analyses and daily 10-day forecasts) with an updated global 1/12° system. In the latter, the ocean/sea-ice model and the assimilation scheme benefit from the following main updates: atmospheric forcing fields are corrected at large-scale with satellite data; freshwater runoff from ice sheets melting is added to river runoffs; a time varying global average steric effect is added to the model sea level; the last version of Gravity field and steady-state Ocean Circulation Explorer (GOCE) geoid observations are taken into account in the mean dynamic topography used for sea level anomalies assimilation; adaptive tuning is used on some of the observational errors; a dynamic height criteria is added to the quality control of the assimilated temperature and salinity vertical profiles; satellite sea-ice concentrations are assimilated; and climatological temperature and salinity in the deep ocean (below 2000 m) are assimilated to prevent drifts in those sparsely observed depths.

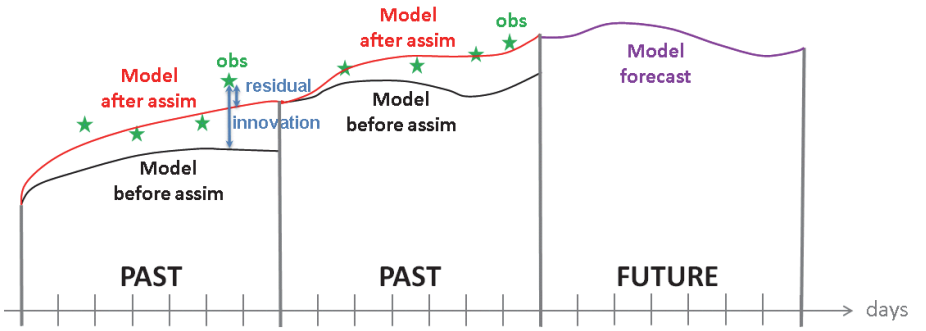


**Figure 20.1.** General principle of an analysis and forecasting system. The model is run a first time and the gap between the observation (green stars) and the model (black line) is called "innovation". An analysis (data assimilation scheme) is done and the model is run a second time, taking into account the correction given by the analysis. The gap between the observations and the model (red line) is then called "residual". Several data assimilation cycles are done in the past to perform the model forecast (purple line) in the future.

This chapter will concentrate on the way the three components of the Mercator Ocean operational system (observation, model, and data assimilation) are integrated to improve the behavior of the system, while maintaining a reasonable elapsed time between the data load and the service delivered to the users. The chapter is organized as follows. The ingredients of the system, with a particular focus on the specifics of the Mercator Ocean, are described first. Technical details about the real-time operation of the system are then given. The next section gives the validation methodology adopted by Mercator Ocean. The system is then examined through a scientific evaluation, highlighting its level of performance and reliability. User needs and evolutions of the system are discussed in the last section.

# Description of the Monitoring and Forecasting System

## Physical model

The high-resolution global analysis and forecasting Mercator Ocean system uses version 3.1 of the NEMO ocean model (Madec et al., 2008). The physical configuration is based on the tripolar ORCA12 grid type (Madec and Imbard, 1996) with a horizontal resolution of 9 km at the equator, 7 km at Cape Hatteras (mid-latitudes) and 2 km toward the Ross and Weddell seas. The 50-level vertical discretization retained for this system has a decreasing resolution from 1m at the surface to 450 m at the bottom, and 22 levels within the upper 100 m. A "partial cells" parameterization (Adcroft et al., 1997) is chosen for a better representation of the topographic floor (Barnier et al., 2006) and the momentum advection term is computed with the energy- and enstrophy-conserving scheme proposed by Arakawa and Lamb (1981). The advection of the tracers (temperature and salinity) is computed with a total variance diminishing advection scheme (Lévy et al., 2001; Cravatte et al., 2007). We use a free surface formulation. External gravity waves are filtered out using the Roullet and Madec (2000) approach. A laplacian lateral isopycnal diffusion on tracers and a horizontal biharmonic viscosity for momentum are used. In addition, the vertical mixing is parameterized according to a turbulent closure model (order 1.5 and mixing length of 30 m) adapted by Blanke and Delecluse (1993). The lateral friction condition is a partial-slip condition with a regionalisation of a no-slip condition (over the Mediterranean Sea) and the elastic-viscous-plastic rheology formulation for the LIM2 ice model (Fichefet and Maqueda, 1997) has been activated (Hunke and Dukowicz, 1997). Instead of being constant, the depth of light extinction is separated in red-green-blue bands depending on the chlorophyll data distribution from mean monthly SeaWiFS (Sea-viewing Wide Field-of-view Sensor) climatology. The bathymetry used in the system is a combination of interpolated ETOPO1 (Amante and Eakins, 2009) and GEBCO8 (Becker et al., 2009) databases. ETOPO1 datasets are used in regions deeper than 300 m and GEBCO8 is used in regions shallower than 200 m, with a linear interpolation in the 200 m – 300 m layer. Moreover, the bathymetry benefits from a specific correction in the Indonesian Sea inherited from the INDESO system (Tranchant et al., 2016).

Internal tide-driven mixing is parameterized following Koch-Larrouy et al. (2008) for tidal mixing in the Indonesian Seas. The atmospheric fields forcing the ocean model are taken from the European Centre for Medium-Range Weather Forecasts' Integrated Forecast System. A three-hour sampling is used to reproduce the diurnal cycle. Momentum and heat turbulent surface fluxes are computed from the Large and Yeager (2009) bulk formulae using the following set of atmospheric variables: surface air temperature and surface humidity at a height of 2 m, mean sea level pressure and wind at a height of 10 m. Downward longwave and shortwave radiative fluxes and rainfall (solid + liquid) fluxes are also used in the surface heat and freshwater budgets. Due to large known biases in precipitations, a satellite-based, large-scale correction of precipitations has been performed, except at high latitudes (poleward of 65°N and 60°S). Moreover, in order to avoid any mean SSH drift due to the large uncertainties in the water budget closure, the following two

treatments were applied. First, a trend of 2.2 mm/year has been added to the runoffs in order to somewhat represent the recent estimate of the global mass addition to the ocean (from glaciers, land water storage changes, Greenland and Antarctica ice sheets mass loss) (Chambers et al., 2017). Second, the surface freshwater budget has been set to zero at each time step with a superimposed seasonal cycle (Chen et al., 2005). The monthly runoff climatology is built with data on coastal runoffs and 100 major rivers from the Dai et al. (2009) database. This database uses data from recent years, streamflow simulated by the Community Land Model version 3 (CLM3) to fill the gaps, in all lands areas except Antarctica and Greenland. In addition, we built the runoff fluxes coming from Greenland and Antarctica ice sheets and glaciers melting using the Altiberg icebergs database project (Tournadre et al., 2013). This complements the estimate of Silva et al. (2006) for Antarctica. Lastly, as the Boussinesq approximation is applied to the model equations, conserving the ocean volume and varying its mass, the simulations do not properly directly represent the steric effect on the sea level (Greatbatch, 1994). For improved consistency with satellite observations of sea level anomalies, which are unfiltered from the steric component, a time-evolving global average steric effect is added to the sea level in the simulation. This global average steric effect has been computed as the time derivative between two successive daily global mean dynamic heights (vertical integration, from the surface to the bottom, of the specific volume anomaly).

## Observations and data assimilation scheme

### Data assimilation scheme

The data assimilation method SAM (Système d'Assimilation Mercator) relies on a reduced-order Kalman filter based on the Singular Evolutive Extended Kalman Filter (SEEK) formulation introduced by Pham et al. (1998). In the Mercator Ocean system, the forecast error covariance is based on the statistics of a collection of three-dimensional ocean state anomalies, typically a few hundred. This approach is based on the concept of statistical ensembles in which an ensemble of anomalies is representative of the error covariances. In our case, the anomalies are computed from a long numerical experiment with respect to a running mean in order to estimate the seven-day scale error on the ocean state at a given period of the year for temperature (T), salinity (S), zonal velocity (U), meridional velocity (V), sea surface height (SSH) and sea ice concentration (SIC). More precisely, each temporal anomaly corresponds to the difference between the model state $M$ and a running mean $\langle M \rangle_{-\tau}^{+\tau}$ over a fixed time period window ranging from $-\tau$ to $\tau$ (Fig. 20.2a).

Moreover, the signal at a few horizontal grid "Δx" intervals in the model outputs on the native full grid is not physical, only numerical (Grasso, 2000). This signal should not be taken into account when updating an analysis. This is why several passes of a Shapiro filter are applied in order to remove the very short scales that, in practice, correspond to numerical noise. Consequently, a little subsampling of the model state is applied without aliasing error and the anomalies are thus calculated on a reduced horizontal grid (one out of every two points in both horizontal directions and all the points along the coast) to limit the storage and the load cost during the analysis stage.

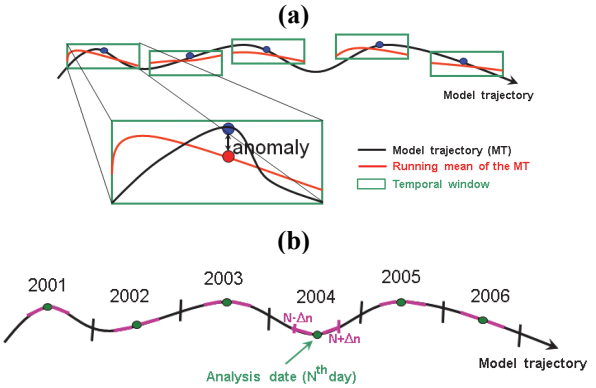


**Figure 20.2**. (a) Schematic representation of the anomalies calculation along a model trajectory and (b) of the use of these anomalies to build the model forecast covariance.

To create the running mean $\langle M \rangle_{-\tau}^{+\tau}$, a Hanning low-pass filter is used:

$$Ha(\nu) = \begin{cases} 0.5 + 0.5\cos\left(\dfrac{\pi.\nu}{\nu_{\max}}\right) & for \quad |\nu| \le \nu_{\max} \\ 0 & for \quad |\nu| > \nu_{\max} \end{cases} \tag{1}$$

where $\nu$ is the temporal frequency of the model state and $\nu_{\max}$ is the cut-off frequency (equal to 1/36 days$^{-1}$ in our case). The main characteristic of the anomaly calculation is to filter out temporal scales at low frequencies in order to keep high frequencies for which the period is shorter than two or three assimilation cycles. For an assimilation cycle centered on the N$^{th}$ day of a given year, ocean state anomalies falling in the window [N-Δn; N+Δn] of each year of the simulation are gathered and define the covariance of the model forecast error (see Fig. 20.2b). In our case, Δn is equal to 45 days, which means that anomalies are selected over 90-day windows centered on the N$^{th}$ day of each year of the simulation. So, in SAM, the forecast error covariances rely on a fixed-basis, seasonally-variable ensemble of anomalies. This method implies that at each analysis step a subset of anomalies is used that improves the dynamic dependency. A significant number of anomalies are kept from one analysis to the other, thus ensuring error covariance continuity. It should also be noted that the analysis increment is a linear combination of these anomalies and depends on the innovation (observation minus model forecast equivalent) and on the specified observation errors. A particular feature of the SEEK formulation is that the error covariance only gives the direction of the model error and not its intensity. An adaptive scheme for the model error variance calculates an optimal variance of the model error based on a statistical test formulated by Talagrand (1998). The last feature of the model forecast covariance employed is a localization technique that sets the covariances to zero beyond a distance defined as twice the local spatial correlation scale. Because a finite number of ocean state anomalies have been used to build the model forecast covariance, the latter is not significant when further away than this particular distance from the analysis point. This is why it is preferable to not use this information and to set the covariance to zero. Spatial (zonal and meridional directions) and temporal correlation scales (Fig. 20.3) are then used to define an "influence bubble" around the analysis point in which data are also selected.

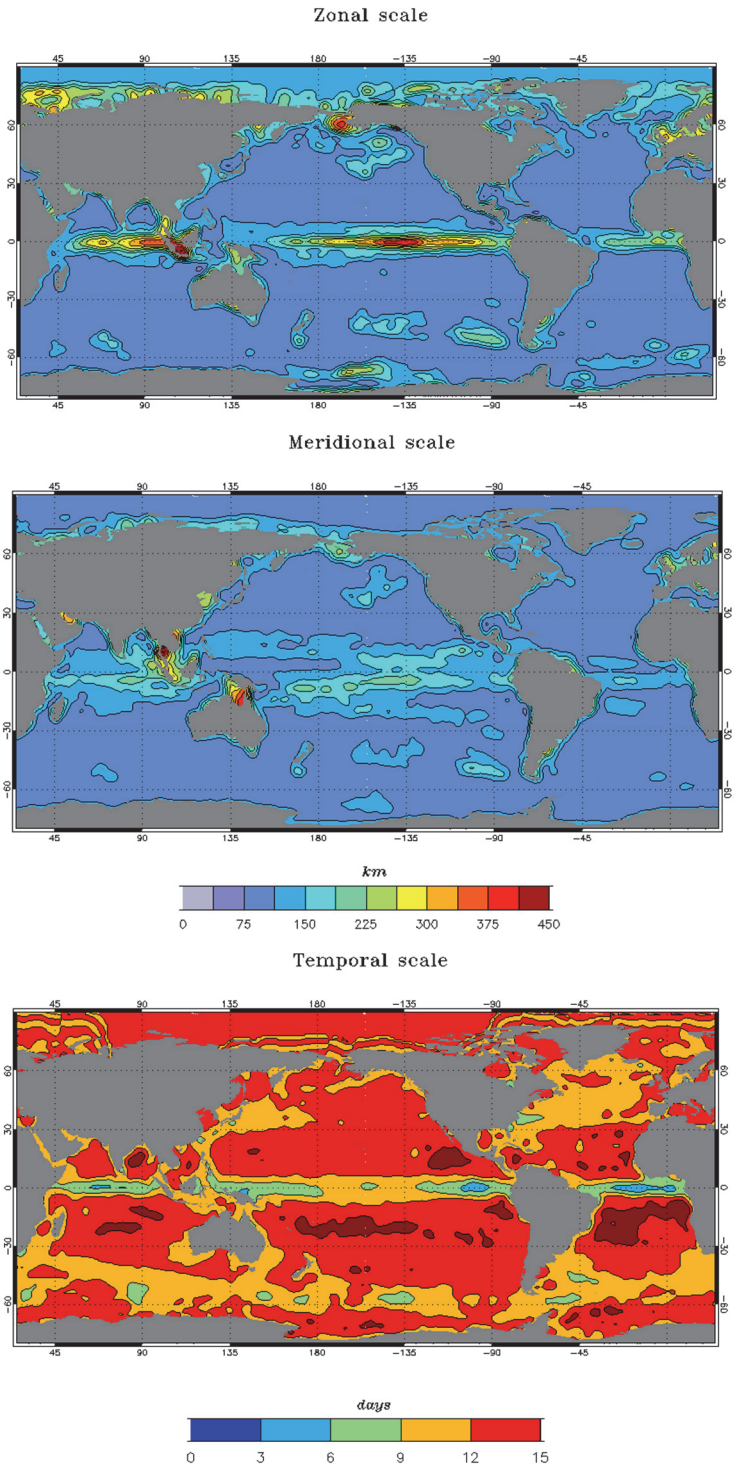


**Figure 20.3**. Zonal, meridional (km), and temporal (days) correlation scales (from top to bottom) used by the Mercator Ocean system.

To save computing time, the analysis is performed on a reduced grid (one out of every four points in both horizontal directions, all the points along the coast and one out of every two points in the first 150 km from the coast). An important distinction of the Mercator Ocean system with respect to more classical forecasting systems is that the analysis is not performed at the end of the assimilation window, but instead at the middle of the seven-day assimilation cycle. The objective is to take into account both past and future information and to provide the best estimate of the ocean centered in time. With such an approach, the analysis, to some extent, acts like a Smoother algorithm.

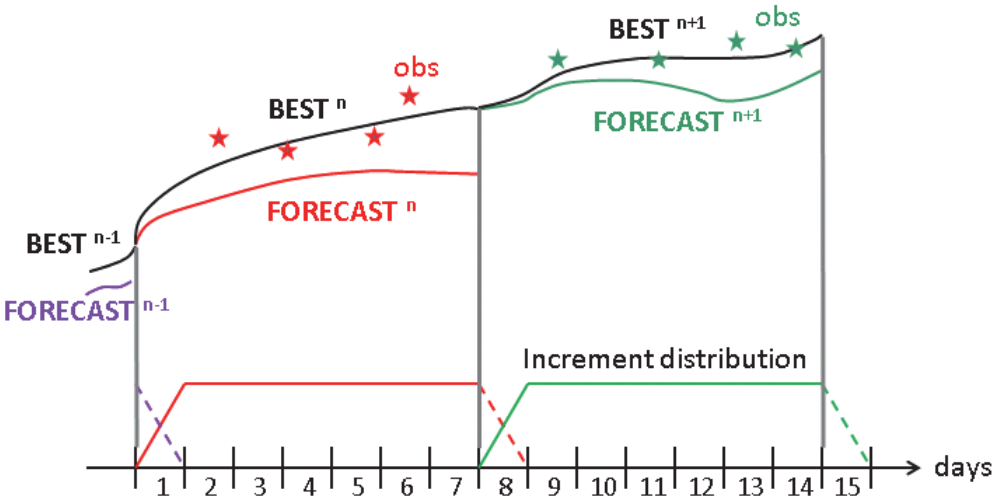


**Figure 20.4.** Schematic representation of the incremental analysis update procedure for three consecutive cycles n-1, n and n+1. Following the analysis performed at the end of the forecast (or background) model trajectory (referred to as "FORECAST" first trajectory, with analysis time at the fourth day of the cycle), the incremental analysis update scheme rewinds the model and starts again from the beginning of the assimilation cycle, integrating the seven-day run (referred to as "BEST" second trajectory) with a tendency term added in the model prognostics equations and modulated by an increment distribution function. The time integral of this function equals one over the cycle length.

After each analysis, the data assimilation produces increments of SSH, temperature, salinity, zonal velocity, meridional velocity, and sea ice concentration. All these increments are applied progressively using the incremental analysis update method (Bloom et al., 1996; Benkiran and Greiner, 2008), which makes it possible to avoid model shock every week due to the imbalance between the analysis increments and the model physics. In this way, the incremental analysis update reduces spin-up effects. Following the analysis performed at the end of the forecast (or background) model trajectory (referred to as "FORECAST" first trajectory, with analysis time at the fourth day of the cycle), a classical forward scheme would continue straight on from this analysis, integrating from day seven until day 14. Instead, the incremental analysis update scheme rewinds the model and starts again from the beginning of the assimilation cycle, integrating the model for seven days (referred to as "BEST" second trajectory) with a tendency term added in the model prognostics equations for temperature, salinity, sea surface height, sea ice concentration, and horizontal velocities. The tendency term (which is equal to the increment divided by the length of the cycle) is modulated by an increment distribution function shown in Fig. 20.4. The time integral of this

function equals one over the cycle length. In practice, the incremental analysis update scheme is costlier than the "classical" model correction (increment applied on one time step) because of the additional model integration ("BEST" trajectory) over the assimilation window.

In addition to this assimilation scheme, a method of bias correction has been developed. This method is based on a 3D-VAR approach, which takes into account cumulative three-dimensional temperature and salinity innovations over the last month in order to estimate large-scale temperature and salinity biases when enough observations are available. The aim of the bias correction is to correct the large scale, slowly-evolving error of the model whereas the SAM assimilation scheme is used to correct the smaller scales of the model forecast error. The bias correction involves several steps. First, temperature and salinity innovations over the last three months are binned and averaged on a coarse resolution (1° x 1°) grid. The two variables are treated separately because temperature and salinity biases are not necessarily correlated. Then, the 3D-VAR method is used to analyze the bias. The bias covariance is constrained by the structures of density fronts in the ocean (the bias can be large on the sides of a front). There is little bias correction in the mixed layer if the vertical gradient of the thermocline is sharp. The bias correction is fully effective under the thermocline, away from density gradients. The correlations are modelled by means of an anisotropic Gaussian recursive filter. Bias correction of temperature, salinity, and dynamic height are then computed and interpolated on the model grid. Lastly, these bias corrections are applied as tendencies in the model prognostic equations, with a one-month timescale.

**Assimilated observations**

Altimeter data, in situ temperature and salinity vertical profiles, satellite sea surface temperature (SST), and sea ice concentration are assimilated to estimate the initial conditions for numerical ocean forecasting. These observations come from CMEMS Thematic Data Assembly Centers, which provide real-time and reprocessed (historic years) satellite and in situ products to be assimilated by the monitoring and forecasting centers.

Altimeter data consist of along-track sea level anomalies (SLA). Along each track of SLA, only one point in two is conserved to avoid redundant information. Moreover, observations along-tracks are smoothed by several altimetric corrections (Le Traon et al., 2001). A mean dynamic topography (MDT) is also used as a reference for SLA assimilation. This MDT is based on the "CNES-CLS13" MDT (Rio et al., 2014) with adjustments made using high-resolution analyses, the last version of the GOCE geoid, and an improved post-glacial rebound (also called a glacial isostatic adjustment). The accuracy of the MDT is very important because it constrains the mean circulation of the model indirectly. For instance, the mean positions of the Gulf Stream, the Kuroshio, or the North Atlantic Current are dictated by the fronts in the MDT. The mesoscale activity given by the SLA is superimposed, but the mean advection is greatly dependent on the MDT.

Temperature and salinity in situ vertical profiles from the CORA 4.1 database (Cabanes et al., 2013) has been assimilated for the hindcast calibration run of the system. This database includes temperature and salinity vertical profiles from the sea mammal database (Roquet et al., 2011) to compensate for the lack of such data at high latitudes. Near real-time satellite operational sea surface temperature and sea ice analysis (OSTIA) SST and the EUMETSAT Ocean and Sea Ice Satellite

Application Facility (OSI-SAF) sea ice concentration are assimilated. For the sea-ice concentration, a separate monovariate/monodata analysis is carried out for the ice variables, in parallel to that for the ocean. The two analyses are completely independent.

Due to unresolved processes and inaccurate forcing, the model may drift at depth. Unfortunately, there are very few temperature and salinity profiles below 2,000 m to constrain the model drift. Hence, the climatology is currently the only source of information at depth to prevent the model from drifting. Virtual vertical profiles of temperature and salinity below 2000m are built from monthly World Ocean Atlas 2013 climatology. These virtual observations are geographically positioned on the model horizontal grid with a coarse resolution (1° x 1°) and on the model vertical levels from 2,200 m to the bottom. A non-Gaussian error is used to impose a weak constraint on the model at depth. This allows the system to capture a potential climate drift at depth.

The concept of "pseudo-observations" or "observed-no change" (innovation equal to zero) is also used to overcome the deficiencies of the background errors, in particular for extrapolated and/or poorly observed variables. We apply this approach to the barotropic height and the three-dimensional coastal salinity at river mouths and all along the coasts (run off rivers). Pseudo-observations are also used for the three-dimensional variables temperature, salinity, zonal velocity, meridional velocity under the ice and between 6°S and 6°N below a depth of 200 m. These observations are geographically positioned on the analysis grid points rather than on a coarser grid in order to avoid generating aliasing on the horizontal. The time of these observations is the same as for the analysis, namely the fourth day of a seven-day assimilation cycle. Given ongoing concern about the need to reduce costs in an operational context, the three-dimensional variables mentioned above were sampled on the vertical in order to keep only about ten model levels.

**Observation operators**

In data assimilation schemes, the computation of innovation requires defining an observation operator to represent the model equivalent of the observation. In the Mercator Ocean system, prognostic variables are interpolated on a quadrilateral grid, i.e., on the four canvas grid points surrounding the observation. The four weights are calculated with a bilinear remapping interpolation.

For in situ vertical profiles, a mapping from the profiles onto the model levels is used. Whenever possible, the nearest data is associated to those levels. In order to prevent large errors near the pycnocline, this procedure is only applied if the data depth is close to the model depth (not further than half the model level thickness). When more than three observations are contained in the in situ profile, a spline algorithm interpolates the profile on the model levels which are in between the observations, only if the distance between the two data depths is less than the model level thickness. No extrapolation is performed at the top or at the bottom of the profile.

For the SST and the sea ice concentration, only the daily data corresponding to the fifth day of the seven-day window is assimilated. For sea ice concentration, the model equivalent corresponds to a simple daily average of the model variable. As OSTIA provides the foundation SST (considered nominally at 10 m depth), the SST model equivalent is performed by calculating the nighttime average of the first level of the model temperature. For SLA, the problem is much more complex.

In order to obtain a consistent model equivalent for SLA, different space/time filters are applied. These time filters act both on the sea level height and the barotropic height computed by the ocean model in order to remove high frequency barotropic signals in a closer manner than what is done in the altimetric data processing (Carrère at al., 2003; Dibarboure et al., 2011). First, the SSH is averaged over a one-day window, and two running means of barotropic height spatially averaged (over a box of 5°) are removed from it.

The model equivalent for SLA is:

$$SLA_{equivalent} = \overline{SSH}_{1day} \text{ - LargeScale } (\overline{HBAR}_{1day} \text{ - } \overline{HBAR}_{21days}) - \text{MDT} \quad (2)$$

The running mean over a one-day window eliminates barotropic high frequencies (periods less than one day) and over a 21-day window eliminates barotropic signals with periods less than 21 days, which correspond to the low-pass filter applied to along-track altimetric data.

Lastly, the First Guess at Appropriate Time (FGAT) method (Huang et al., 2002) is used, which means that the forecast model equivalent of the observation for the innovation computation is taken at the time for which the data are available, even if the analysis is delayed.

**Quality control on in situ observations and feedback to input data providers**

To minimize the risk of erroneous observations being assimilated in the model, the system carries out two successive quality controls (QC1 and QC2) on the assimilated temperature and salinity vertical profiles. These are done in addition to the quality control procedures performed by the data producers.

*Quality Control (QC1)*

QC1 allows the detection of spikes and large biases. It can be summarized as follows. An observation is considered suspicious if the following two conditions are satisfied:

$$\begin{cases} |innovation| > threshold \\ |observation - climatology| > 0.5 * |innovation| \end{cases} \quad (3)$$

where the spatially and seasonally varying $threshold$ value comes from statistics (mean, standard deviation) computed with the very large number of temperature and salinity innovations collected in GLORYS2V1 Mercator Ocean reanalysis (1993-2009). The first condition is a test on the innovation. It determines whether the innovation is abnormally large, which would most likely be due to an erroneous observation. The second condition avoids rejecting “good” observations (i.e., an observation close to the climatology) even if the innovation is high due to the model background being biased. Fig. 20.5 shows an example of a wrong temperature profile detected by the quality control in the GLORYS2V1 simulation. Below 400 m in depth, innovations are no longer valid. The two conditions described previously are satisfied and the profile is rejected (Fig. 20.5a). When this profile is assimilated, an abnormal salinity value appears at its temporal and geographical positions (Fig. 20.5b). This is due to the fact that the assimilation algorithm used is multivariate, meaning that an observation of temperature leads to corrections of all of the model variables and especially, in this case, the surface salinity.

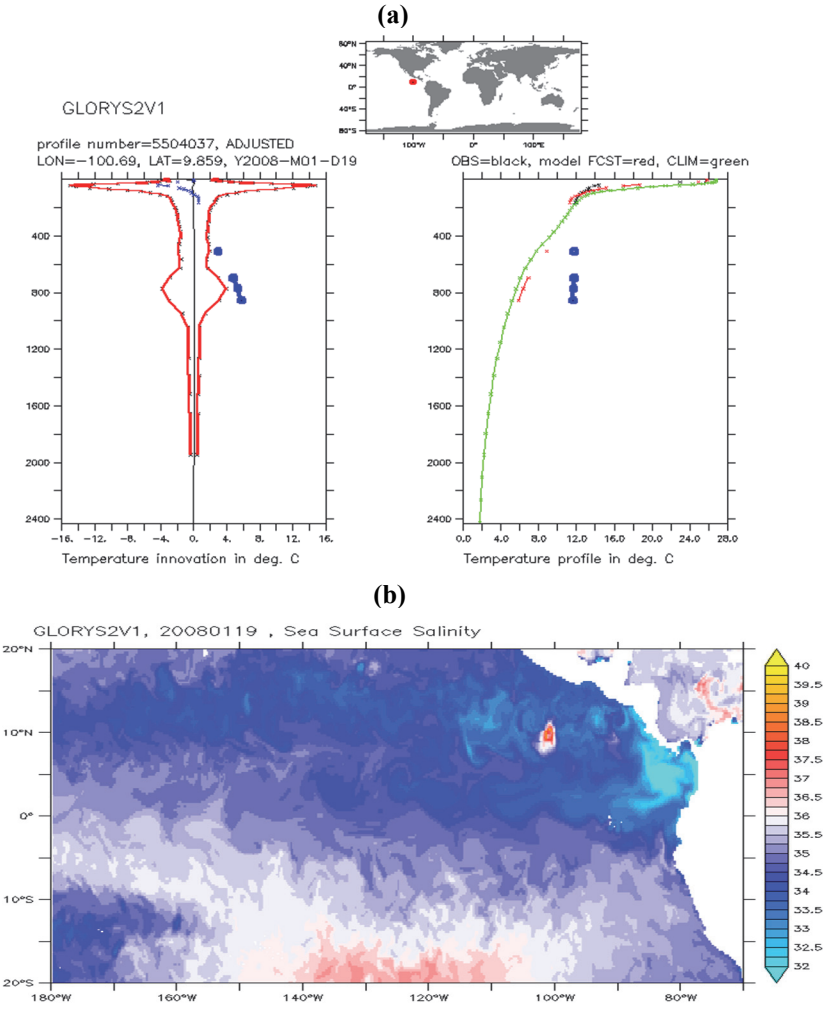


**Figure 20.5**. Example of a suspicious temperature vertical profile at 100.69° W - 9.86° N, highlighted by the quality control on the CORA3.1 dataset. **(a)** Left panel shows temperature innovation profile in blue and temperature innovation threshold in red. Right panel shows the absolute vertical temperature profile (observation in black, climatology in green and model in red). Large blue dots correspond to "bad" innovations or "bad" observations. **(b)** When this profile is assimilated, an abnormal value of salinity appears at the position of this profile.

*Quality Control (QC2)*

QC2 is based on dynamic height innovation statistics and allows detection of small biases, which are present in the whole water column and thus can induce large errors. It basically says that the thermosteric or halosteric information cannot exceed some threshold in height. It can be summarized as follows.

An observation is considered to be suspect if:

$$\begin{cases} For\ temperature: \dfrac{|C*hdyn(innov_T)|}{\sum dz_T} > threshold_T \\ For\ salinity: \dfrac{|C*hdyn(innov_S)|}{\sum dz_S} > threshold_S \end{cases} \quad (4)$$

$$\text{where} \quad \begin{cases} C = 200/\sum dz \;\; if \;\; 0 < \sum dz \leq 200 \\ C = 500/\sum dz \;\; if \;\; 200 < \sum dz \leq 500 \\ C = \sum dz \;\; if \;\; \sum dz > 500 \end{cases} \tag{5}$$

and $\boldsymbol{dz_T}$ is the model layer thickness corresponding to the temperature observation (same for $\boldsymbol{dz_S}$ and salinity). These last conditions (Eq. 5) prevent the $threshold$ from being reached too quickly in shallow areas.

The parameters used by QC2 (average and standard deviation of the dynamical height innovations, and therefore threshold value) have been calculated from a global simulation at 1/4°, which is a twin simulation of the high-resolution one. Note that the simulation at 1/4° also assimilates the CORA 4.1 CMEMS in situ database. The threshold two-dimensional field is then computed as the average plus six times the standard deviation of the dynamical height innovations (Fig. 20.6).

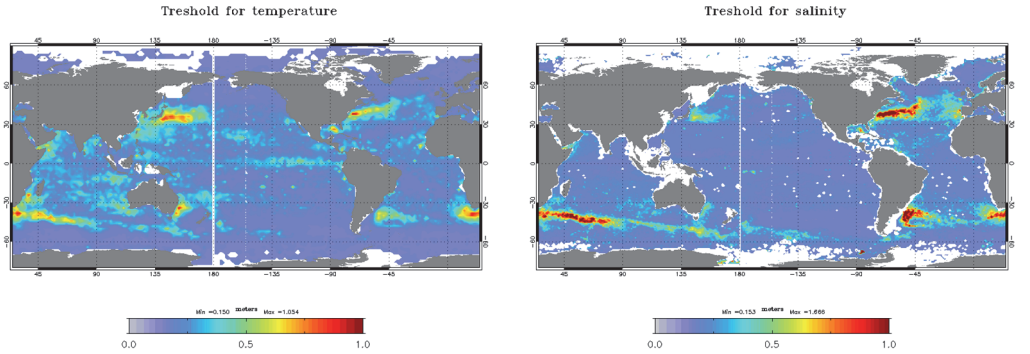


**Figure 20.6.** Threshold used for QC2 for temperature (left panel: $threshold_T$) and salinity (right panel: $threshold_S$).

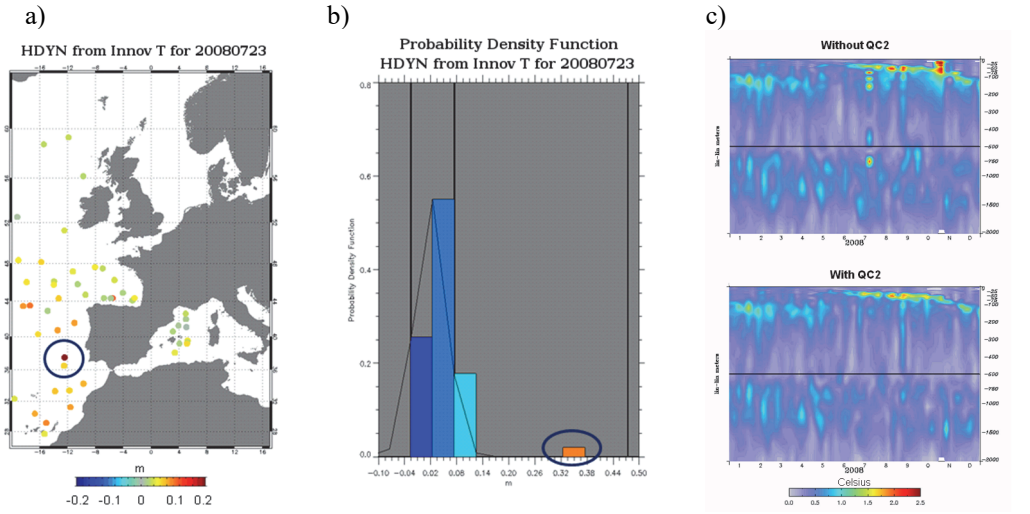


**Figure 20.7.** Statistics in the Azores region: a) absolute value of dynamical height innovations from temperature innovations for the 7-day assimilation cycle from 16 July 2008 to 23 July 2008, b) Probability density function (PDF) of theses dynamical height innovations (the value 0.3 appears in the tail of the PDF), c) Root mean square (RMS) innovation with respect to the vertical temperature profiles over the year 2008 for two "twins" simulations (without and with QC2). These last scores are averaged over all seven days of the data assimilation window, with a lead time equal to 3.5 days.

Fig. 20.7a shows an example of a "wrong" temperature profile detected by the QC2 at the end of July 2008. In this case, $threshold_T = 0.3$ (Fig. 20.7b). The first condition of Eq. 4 is satisfied and the profile is rejected. When this profile is assimilated (simulation without QC2), abnormal temperature root mean square (RMS) innovation values appear at the temporal position (July 2008) of this profile in the Azores region (Fig. 20.7c). Using QC2 quality control allows for solving the problem.

**Adaptive tuning of observation error and implementation**

In order to refine the prescription of observation errors, adaptive tuning of observation errors for the SLA and SST has been implemented. The method has not been used for temperature and salinity vertical profiles because of the lack of in situ data. Then, three-dimensional fixed observation errors are used for the assimilation of in situ temperature and salinity vertical profiles. These three-dimensional errors have been computed from the last MyOcean global 1/4° Mercator system using an offline version of the adaptive tuning method mentioned above. Fig. 20.8 shows these observation errors at surface and at 100 m depth.

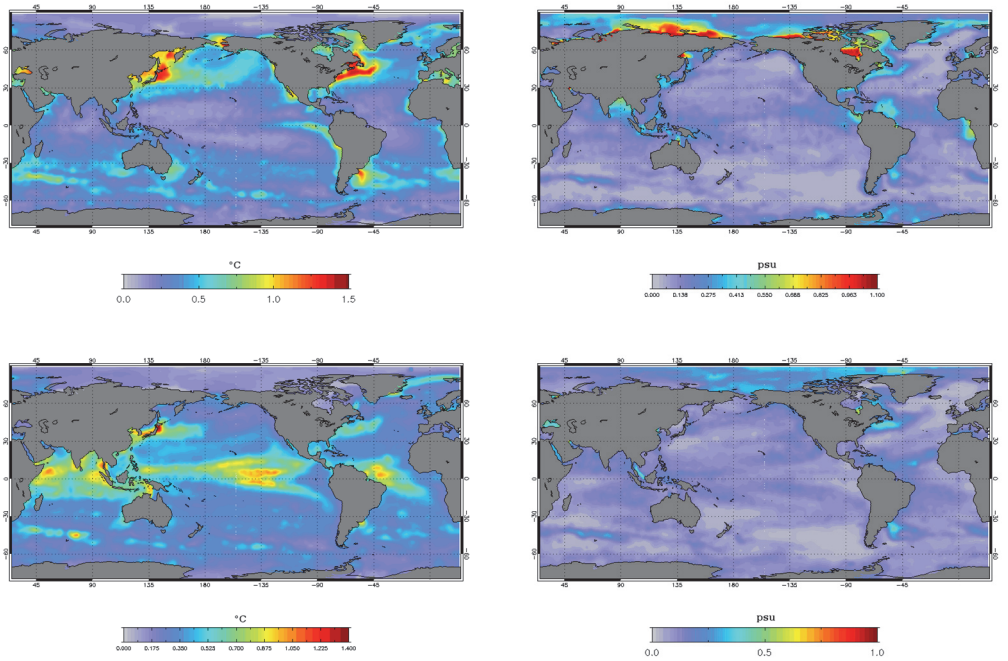


**Figure 20.8.** Observation errors used in SAM for in situ temperature (left panels) and salinity (right panels) profiles, at surface (top) and at 100 m depth (bottom).

The adaptive tuning method consists in the computation of a ratio, which is a function of observation errors, innovations, and residuals. It helps correct inconsistencies on the specified observation errors. Following Desroziers et al. (2005), this ratio can be expressed as:

$$ratio = \frac{residual\ (innovation)^T}{observation\ error} \tag{6}$$

Ideally, $ratio$ is equal to one. When the ratio is less (respectively larger) than one, it means that the observation error is overestimated (respectively underestimated). The objective of this diagnostic is to improve the error specification by tuning an adaptive weight coefficient acting on the error of each assimilated observation. As a first guess of the method, the initial prescribed observation error matches the one used in the previous system (Lellouche at al., 2013), where the observation error variance was increased near the coast and on the shelves for the assimilation of SLA, and increased only near the coast (within 50 km of the coast) for the assimilation of SST. Only an illustration of the method on the SLA is shown here. Similar results are obtained for SST. Fig. 20.9 represents the temporal evolution of the ratio for Envisat satellite. At the beginning of the simulation, the observation error is overestimated (ratio less than one). The ratio tends to one after only a few weeks of simulation.

For SLA (Fig. 20.10), the a priori prescribed observation error is globally significantly reduced. The median value of the error changed from 5 cm to 2.5 cm in a few assimilation cycles and allows for better results. This method allows us to have more realistic and evolutive observation error maps which can provide valuable information to space agencies.

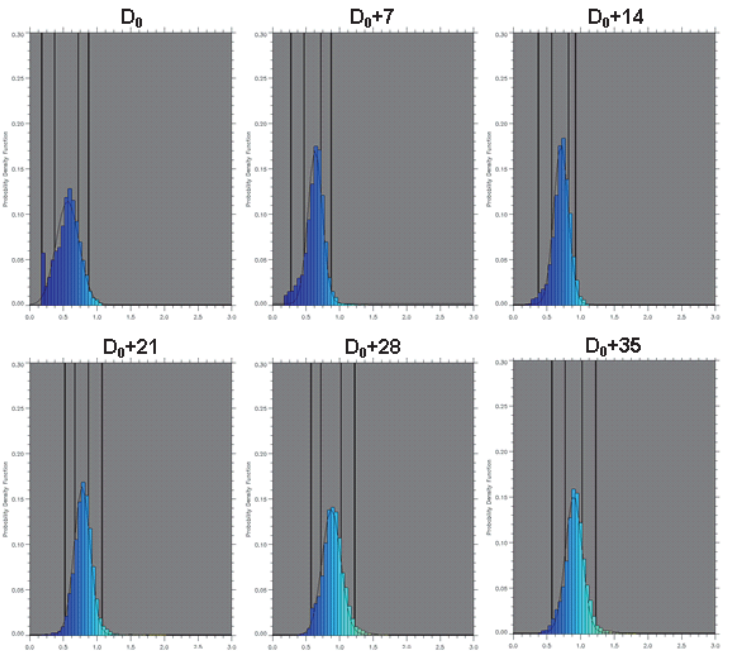


**Figure 20.9.** Evolution of the PDF of the ratio for Envisat satellite. $D_0$ corresponds to the first day where Envisat is assimilated by the system.

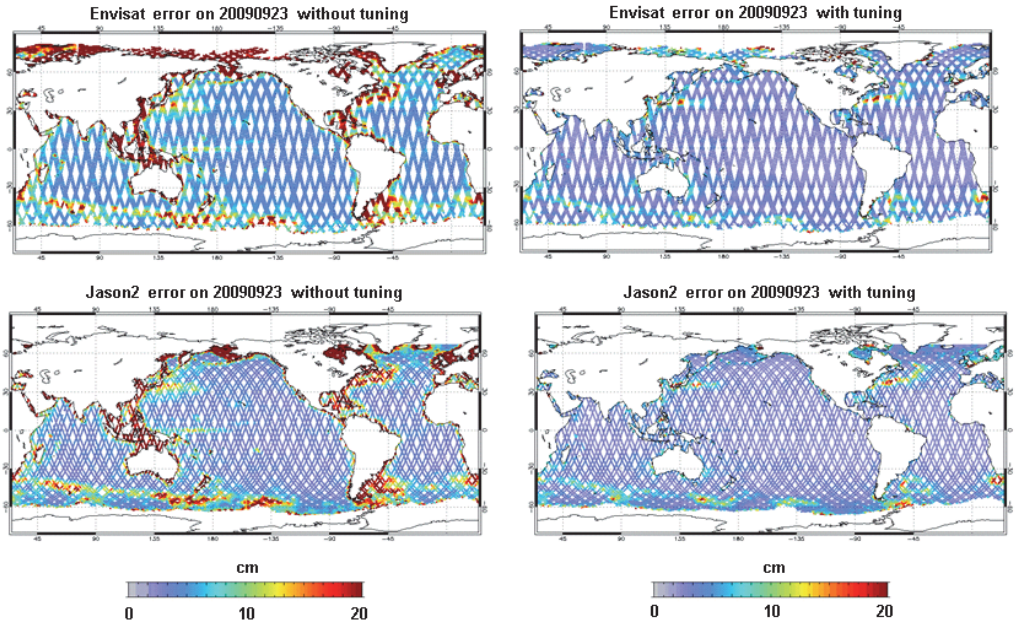


**Figure 20.10.** Envisat (top panels) and Jason2 (law panels) observation errors used on seven-day assimilation cycle ending September 23, 2009 without tuning (left panels) and with tuning (right panels) method.

## Real-time Operation of the System, Computing Facility, Dissemination Capacity and Service Delivery

The system is run weekly on Wednesdays and provides two weekly analyses and two weeks of forecast (Fig. 20.11). The first analysis (hindcast) is the better one and is performed 14 days behind the real-time (from D-14 to D-8 included). The second analysis (nowcast) is performed seven days behind the real-time (from D-7 to D-1 included). Moreover, each day, the system is run without assimilation for days D-1 to D+9, providing ten days of forecast by updating the atmospheric forcing of the first day. The daily runs are initialized with the previous day's run, except on Thursdays, when they start from the weekly analysis run.

The system runs on 54 nodes (1296 processors) of Météo France BULL machine. The ocean model alone takes one hour (elapsed time) for a seven-day simulation and the analyses (SEEK and 3D-VAR) take 0.6 h. This means a total of about eight hours elapsed (two analyses, 42 model days, and computation of diagnostics) every week to deliver the 14-day forecast. This illustrates the fact that computing resources remains a key limiting factor to the development of global high resolution systems to be able to deliver the service to users within a reasonable time.

Moreover, the system generates a huge amount of data (0.5Tb per week) that have to be physically stored to provide the services. The storage capacity is important, but even more important is the question of efficient access to the data stored by the users in a timely manner. To address this issue, the web server “Motu” is used, which allows for the distribution of met/ocean gridded data files through the web. Motu is a highly efficient and robust software tool that fills the gap between

heterogeneous data providers to end users and allows for handling, extracting, and transforming oceanographic huge volumes of data without performance collapse. Lastly, a service desk has been put in place to help users with the products, register the requests, and make sure that the service is well-delivered.

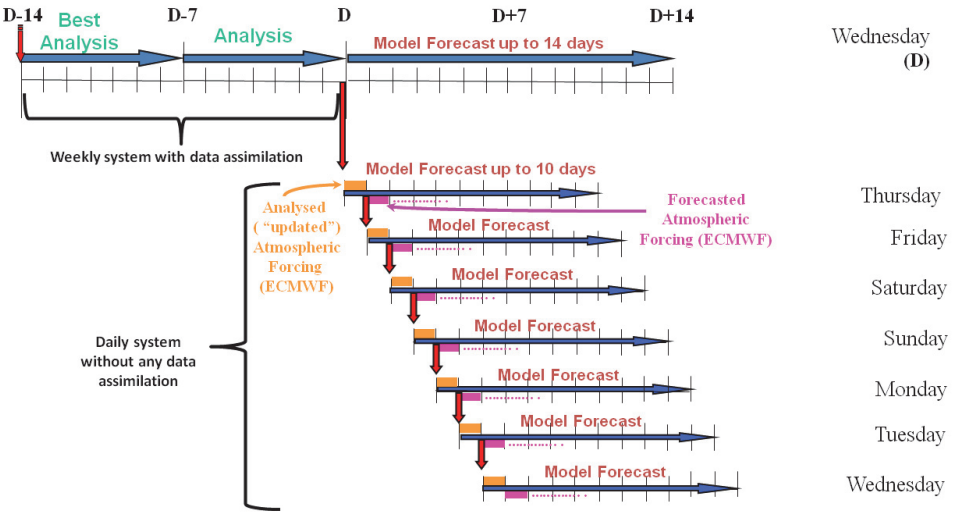


**Figure 20.11.** Schematic representation of the operational schedule for operation of the system. Real-time corresponds to the base date D. Vertical arrows in red represent the writing of files allowing to the model to restart.

## Validation Methodology

### Metrics and calibration period

Scientific quality is one of the key criteria for the continuous improvement of CMEMS products. Moreover, metadata on scientific quality helps users understand the content of products and their usefulness. Therefore, it is very important for monitoring and forecasting centers to agree on quality standards and to produce homogeneous and accessible information on the scientific quality of their analyses and forecasts. The scientific assessment procedure applied for CMEMS consists of two phases. During the first "calibration phase," new products or developments are checked with a series of metrics before being commissioned. Once the product has been commissioned it then undergoes an "operational validation phase" during which the products are checked against the reference calibration results. Standards and metrics were defined during the MERSEA (Marine Environment and Security for the European Area) integrated project and in the context of GODAE. These standardized diagnostics have enabled comparative exercises between European operational oceanography monitoring and forecasting centers (Crosnier and Le Provost, 2007) and others outside of the EU (Hernandez et al., 2009).

Some of these metrics were proposed for calibration and validation purposes. An efficient validation procedure has already been defined by Mercator Ocean for its model, including scientific

assessment (calibration) and quarterly control bulletins (validation). These documents give a general picture of the normal behavior of the system in terms of accuracy and realism of the ocean physics. The accuracy is measured by the differences between simulations and observations and the realism by studying particular oceanic processes. In addition, more than a thousand diagnostic checks are routinely performed every day at Mercator Ocean.

The metrics that can be divided into four main categories derived from Crosnier and Le Provost (2007). The consistency between two-system solutions or between a system and observations can be checked by "eyeball" verification. This consists in comparing subjectively two instantaneous or time mean spatial maps of a given parameter. Coherent spatial structures or oceanic processes such as main currents, fronts, and eddies are evaluated. This process is referred to as CLASS1 metrics. The consistency over time is checked using CLASS2 metrics, which include comparisons of moorings time series, and statistics between time series. Space and/or time integrated values such as volume and heat transports, heat content, and eddy kinetic energy are referred to as CLASS3. Their values are generally compared with literature values or values obtained with past time observations such as climatologies or reanalyses. Finally, CLASS4 metrics give a measure of the real-time accuracy of systems by calculating various statistics of the differences between all available oceanic observations (in situ or satellite) and their model equivalent at the time and location of the observation.

The scientific assessment or calibration procedure thus involves all classes of metrics. It checks improvements between versions of a system, and ensures that a version is robust and its performance stable over time. The assessment must be conducted through a one-year numerical experiment at least, in order to obtain representative results. It is currently very difficult to run real-time systems over many years in the past, for computational reasons, but also due to the recent (and ongoing) evolution of the ocean observational network. Different data densities imply different tunings of the data assimilation system.

## Quality check of real-time analyses and forecasts

Once the scientific assessment has been done and the system's nominal accuracy values and consistent behavior have been described, it is possible to apply a regular quality check to the real-time analyses and forecasts. Due to the very large amount of information produced by a global system, a real-time quality check is based on a reduced number of metrics, and comparisons with observations are constrained by their availability and timeliness. However, more than a thousand graphics are checked each week (weekly monitoring of the analysis) and each day (consistency check of the daily forecast) by Mercator Ocean. The major part of this procedure is currently being automated with indicators based on distribution (percentiles) thresholds computed from the scientific assessment stage. To record the strengths and weaknesses of forecasting systems, Mercator Ocean has published the Quarterly Ocean Validation Bulletin "*QuO Va Dis?*" since July 2010. It is available at http://www.mercator-ocean.fr/eng/science/qualification. There, one can find observation minus analysis (called "residual") and observation minus forecast (called "innovation") statistics for temperature and salinity vertical profiles, SST, SLA, and sea ice concentration

observations that are assimilated. Comparisons are also made with independent observations, such as currents at 15 m derived from drifting buoys, sea-ice drift, or tide gauges (the low frequency component of the tide gauges' elevation signal). Integrated parameters such as sea ice extent and global mean SST are monitored. Process studies focusing on one process or region, or short research and development validation studies complement the bulletins.

In the next section, we illustrate the scientific assessment results mostly with the same metrics.

## Assessment of the System

This section describes the Mercator Ocean system's quality assessment with diagnostics over particular years, assorted with time series over multiyear periods. To give an idea of the quality of the system, the distance to the assimilated observations (SST, SLA, temperature and salinity vertical profiles, and sea ice concentration) is measured. Moreover, the analyses are also compared with observations that have not been assimilated by the system.

### SST

**Assimilation diagnostics**

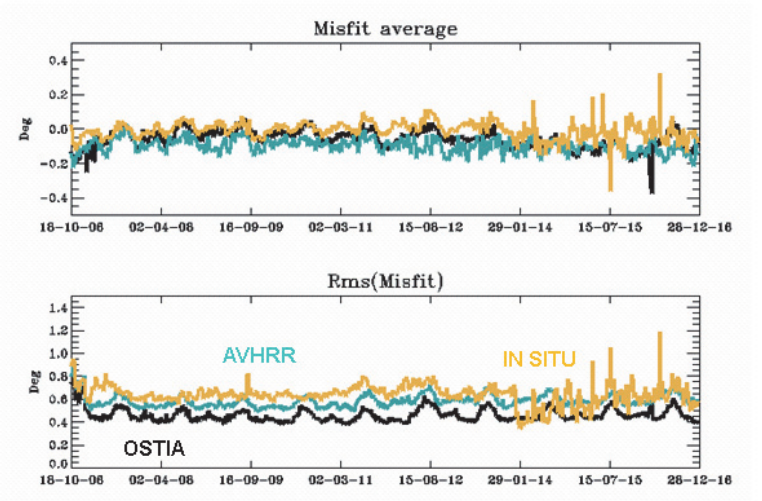


**Figure 20.12.** SST (°C) global misfit average (top) and RMS (bottom) for OSTIA observations (black line, assimilated), NOAA AVHRR observations (blue line, not assimilated), and in situ observations (orange line, assimilated), for the (October 2006 - December 2016) hindcast period.

Here we checked temporal series of the mean and the RMS of the misfit between the observed SST and the model. For OSTIA SST, we obtain a mean warm bias of -0.1°C and a mean error of 0.45°C (Fig. 20.12). Seasonal fluctuations of the SST biases on a global average can be seen as a lack of stratification in the model, which causes stronger mid-latitude cold biases during (boreal) summer (and a warm bias between 50 m and 100 m). For in situ SST, the bias is smaller, suggesting that OSTIA might be colder than in situ near surface observations on global average. We can notice a drop in the RMS of in situ surface data at the end of the period, which is due to the use of near real-

time observations, where most of the surface observations do not have sufficient quality flag (drop in the number of data).

**SST mode decomposition**

An empirical orthogonal function (EOF) analysis is used to assess the variability of the SST over the time period 2010-2014. An EOF decomposition for the system (hindcast period) and the OSTIA SST has been performed.

Fig. 20.13 shows the mode 3 corresponding to the ENSO signal, which is very faithfully reproduced by the system. The SST EOFs are very robust and there are very few differences between the system and the observations up to mode 10. The only differences concern the coastal structures that are sharper with the system.

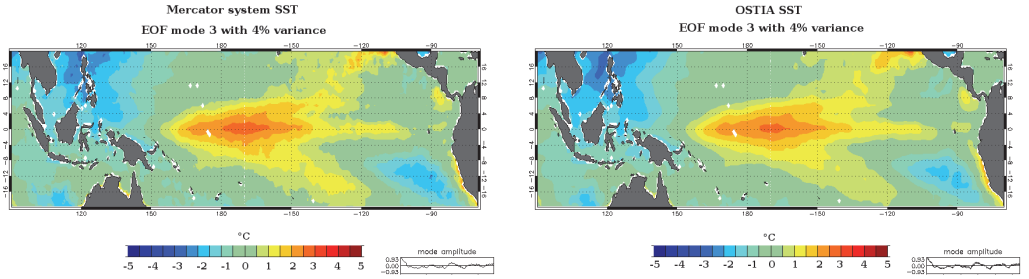


**Figure 20.13.** 3th EOF (bottom panel) of SST (°C) over the time period 2010-2014 (left panel: model SST, right panel: OSTIA SST). The time series at the bottom of each panel correspond to the mode amplitude.

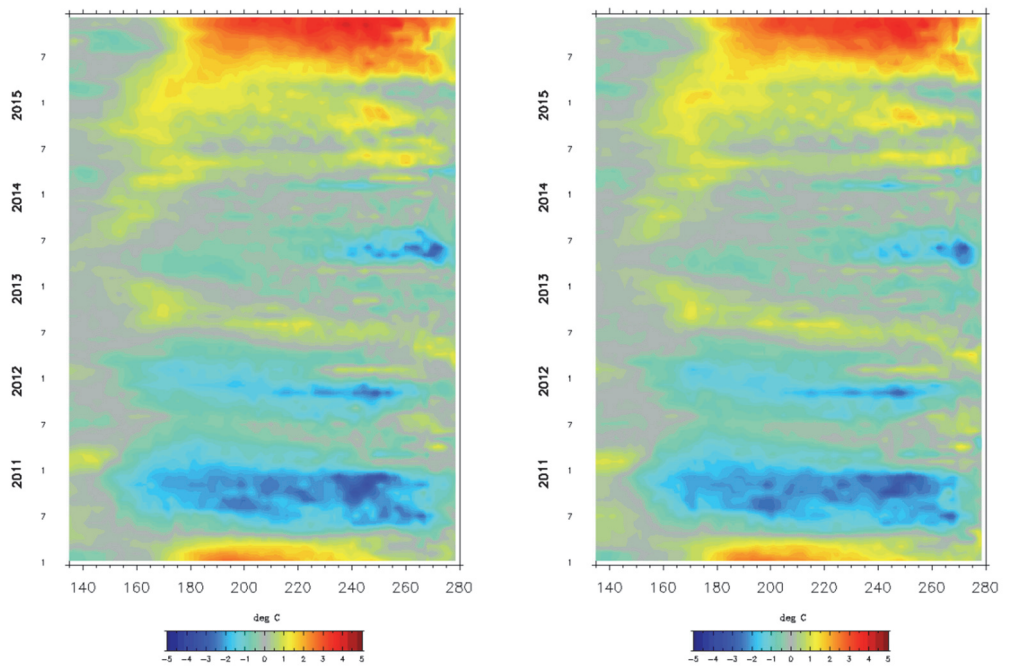


**Figure 20.14.** SST longitude time diagrams within 2°N-2°S over the Pacific (left panel: model; right panel: OSTIA observation). Monthly anomalies relatively to the 2010-2015 seasonal signal.

**Equatorial propagation**

The 2010-2015 monthly anomalies averaged within 2°N-2°S are used to validate the equatorial propagation with the SST.

Fig. 20.14 shows the coherence between the system and the OSTIA SST, both in terms of amplitude and phase. There is a little westward shift in longitude of the system structures, but the equatorial propagation can be seen in the system and the observations. Following the 2010-2011 La Niña, the westward propagation of the warm anomaly is clear in the system and the observation (second half of 2012). The equatorial slope returns to normal in 2013 and warm waters accumulate in the west. The El Niño that did not quite happen is visible in winter 2013-2014 in the west. The eastward Kelvin wave in May-June 2014 warms the eastern side and reflects into a westward Rossby wave. This reinforces the 2015 El Niño warming east of the dateline.

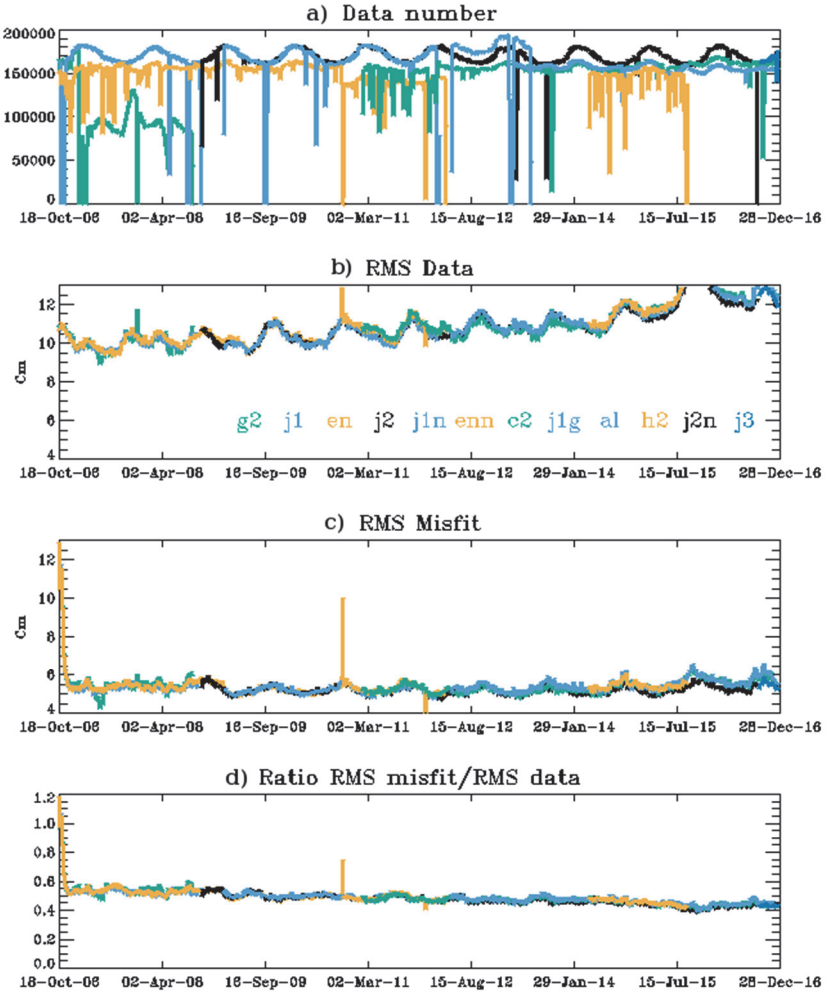


**Figure 20.15.** Time evolution of SLA (cm) data assimilation statistics averaged over the whole domain: a) data number, b) quadratic mean of the SLA data, c) RMS of innovations, d) RMS of innovations divided by quadratic mean of SLA observations. The scores are averaged aver all seven days of the data assimilation window, with a lead time equal to 3.5 days.

## Sea level anomalies (SLAs)

### Assimilation diagnostics

Fig. 20.15 shows time series of assimilation statistics. The system is close to altimetric observations with a forecast RMS difference of the order of 5.5 cm. It does better than the previous system, which had a forecast RMS difference of the order of 6.5 cm. This is mainly due to the use of the "Desroziers" method to adapt the observations errors online, which yields to more information from the observations being used. Moreover, the model is able to explain the observed signal as shown by the ratio of RMS innovation to RMS data, which decreases with time and converges towards a value less than one.

Fig. 20.16 illustrates the skill related to the different changes of versions of the global system. For this figure, only statistics with Jason1 (J1), Jason2 (J2), and Jason3 (J3) altimeters are shown. The improvement between successive versions can be seen thanks to the increase of horizontal resolution (from 1/4° to 1/12°) and to refinements or adjustments to the system (model and data assimilation updates).

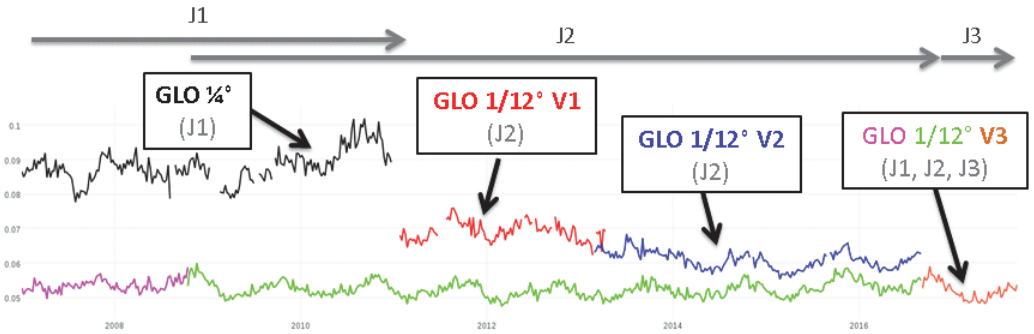


**Figure 20.16.** Time evolution of RMS of SLA innovations (m) related to the different changes of versions of global systems at ¼° or 1/12° resolution. Only statistics with Jason1 (J1), Jason2 (J2), and Jason3 (J3) altimeters are shown. Early performances were about 10 cm whereas they are now close to 5 cm.

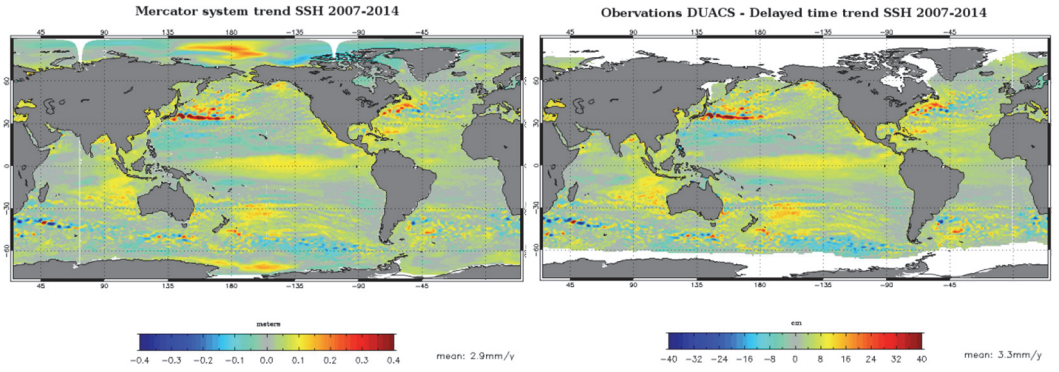


**Figure 20.17.** Model (on the left) and observations (on the right) SSH trends over the time period 2007-2014.

### SLA trends

Next, we compare the sea level trends from the system and the Data Unification and Altimeter Combination System (DUACS) delayed time SLA for the time period 2007-2014 in order to avoid the signature of the strong 2015 El Niño. Fig. 20.17 shows good spatial agreement between the system and the data. The shift in global mean sea level (2.9 mm/year for the system and 3.3 mm/year for the data) is due to the glacial isostatic adjustment (0.3 mm/year), which must be added to the ocean model.

### SLA mode decomposition

Next, we compare the EOF decomposition of the SLA from the system and data for the time period 2000-2014. Again, the EOFs are very similar in terms of spatial patterns and time amplitudes up to mode 10. Fig. 20.18 shows this property for mode 4. It corresponds to the extinction of the 2010-2011 La Niña (the amplitude is negative at the beginning). The joined effect on the equatorial SST can be seen in Fig. 20.14.

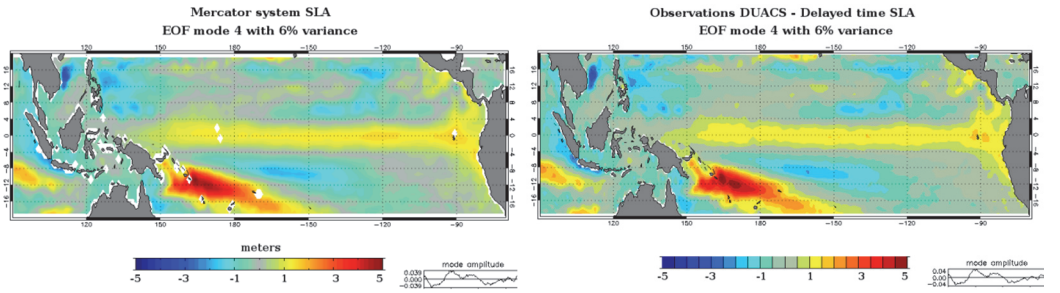


**Figure 20.18.** Fourth EOF (bottom panel) of SLA (m) over the time period 2010-2014 (left panel: model SLA, right panel: DUACS SLA). The time series at the bottom of each panel correspond to the mode amplitude.

## Temperature and salinity vertical profiles

Next, we check time series of the RMS of the difference between the model analysis and the observations, for temperature on the left and for salinity on the right (Fig. 20.19) in the whole water column. We compare observation and climatology (red line), the previous system (blue line), and the current system (black line).

On global average, the current system slightly degrades the temperature statistics (-0.03°C) but greatly improves the salinity statistics (+0.1 psu). This enables us to get a more accurate description of the water masses and better balance arises from the new in situ errors that give more weight to the salinity data. Note that the systems are always better than the climatology.

The current system experiences a slight warm bias (negative observation – forecast difference) in subsurface (25-500 m) on global average (not shown). For the year 2015, part of this signal comes from the strong interannual ENSO signals in the Tropical Pacific, where the near-surface bias is also warm, as well as in the Antarctic Circumpolar Current and the Gulf Stream. Seasonal cold surface biases appear in the mid latitudes, linked with a lack of stratification during summer. Summer warming is injected too deep which results in subsurface spurious warming and a mixed layer that is too shallow. However, these biases remain small on global average.

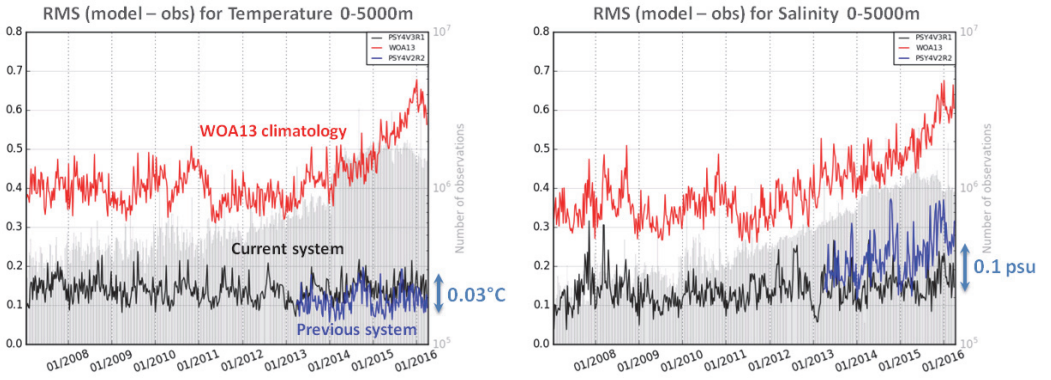


**Figure 20.19.** Time series of the RMS of the difference between the model analysis and the in situ observations (in the whole water) column for previous and current systems and the World Ocean Atlas 13 climatology. Left panel: temperature (°C), right panel: salinity (psu). Time series of the number of available observations appear in grey.

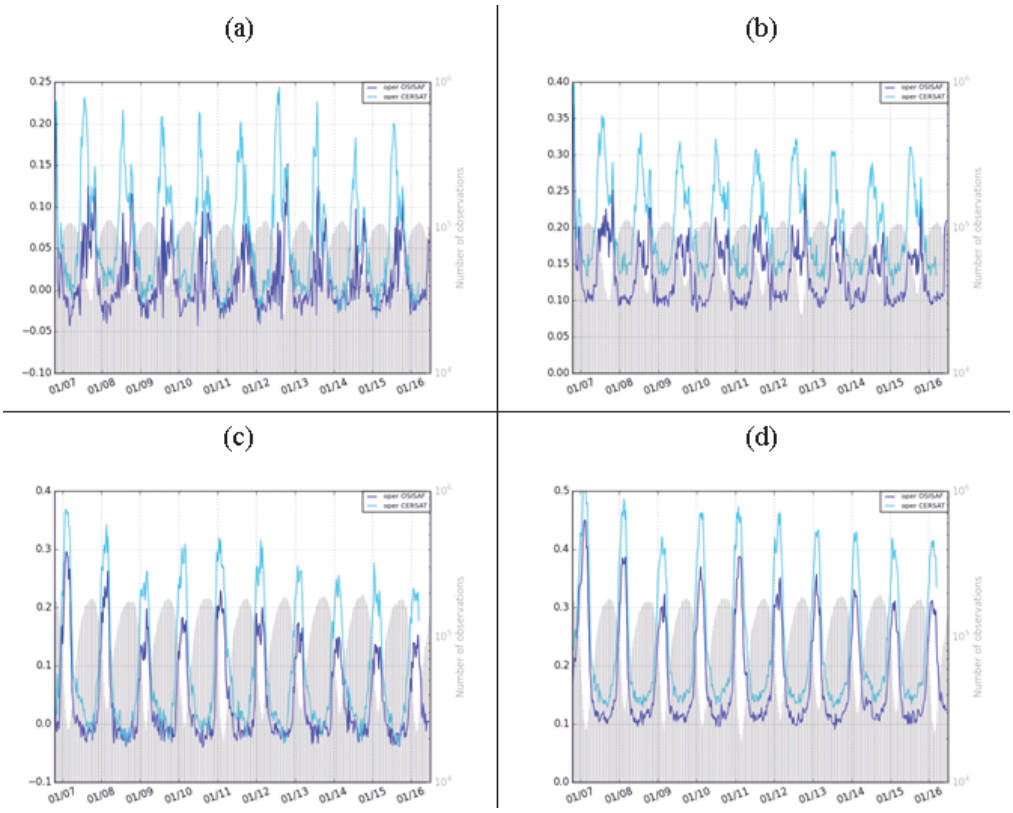


**Figure 20.20.** (observation-forecast) mean (a and c) and RMS (b and d) differences of sea ice concentration (0 means no ice, 1 means 100% ice cover) in the Arctic Ocean (a and b) and Antarctic Ocean (c and d) over the time period 2007-2016. Dark blue is the mean or RMS error of the system with respect to assimilated OSI Thematic Data Assembly Centers' sea ice concentration, light blue is the mean or RMS of the system with respect to CERSAT sea ice concentration observations. Time series of the number of available observations appear in grey.

## Sea ice concentration

As shown in Fig. 20.20, the system sees slightly too much ice during the beginning of the melting season in summer (up to 3% overestimation on average in both the Arctic and Antarctic basins), while the mean error is stronger on average during winter (10-20% underestimation, depending on the year). RMS errors are also larger during the summer melt season (up to 20% in the Arctic and up 30% in the Antarctic with respect to OSI Thematic Data Assembly Centers' observations), and they drop to less than 10% in winter. These RMS errors quantify the capacity of the system to capture weekly time changes in the ice cover. In the Arctic, the error peaks without data assimilation occur at the sea ice cover minimum in September, while the error peaks with data assimilation occur earlier in July-August when the sea ice melts. This may be linked to the fact that the weekly assimilation of sea ice concentration is not fitted to constrain rapid changes in the sea ice cover in the marginal seas.

## Currents

In this section, we use velocity observations that were not assimilated in the system or a case study to assess the level of performance of the current system compared to the previous ones.

**Drifter velocities: near surface validation**

The 15 m currents are checked by comparing the model to velocity observations coming from Argo surface floats and in situ Atlantic Oceanographic and Meteorological Laboratory drifters. Grodsky et al. (2011) revealed that an anomaly in the drogue loss detection system of the Surface Velocity Program buoy had led to the presence of undetected undrogued data in the "drogued-only" dataset distributed by the Surface Drifter Data Assembly Center. Rio (2012) applied a procedure using altimeter and wind data to produce an updated dataset, including a wind slippage correction. Therefore, we use this new in situ dataset coming from CMEMS Thematic Data Assembly Centers to check mean model currents. The "YoMaHa" real-time surface ARGO drifts are utilized, as well (Lebedev, 2007).

Fig. 20.21 shows a comparison of the 2007-2015 averaged drifts from the system and the observations over the Indonesian region. Currents in this region are very difficult to resolve because of the many narrow straits and strong tidal mixing. The retroflection of the westward South and North Equatorial Currents (along Papua and near 12°N) into the eastward North Equatorial Counter Current (near 4°N) are well-reproduced structures in the Pacific. The system South Equatorial Current is a little too strong at the edge of the warm pool. The complex flow in the Sulawesi Sea, the Makassar Strait and the South China Sea is also well-reproduced by the system. The correlation is 0.70 (respectively 0.64) for the zonal (respectively meridional) velocity.

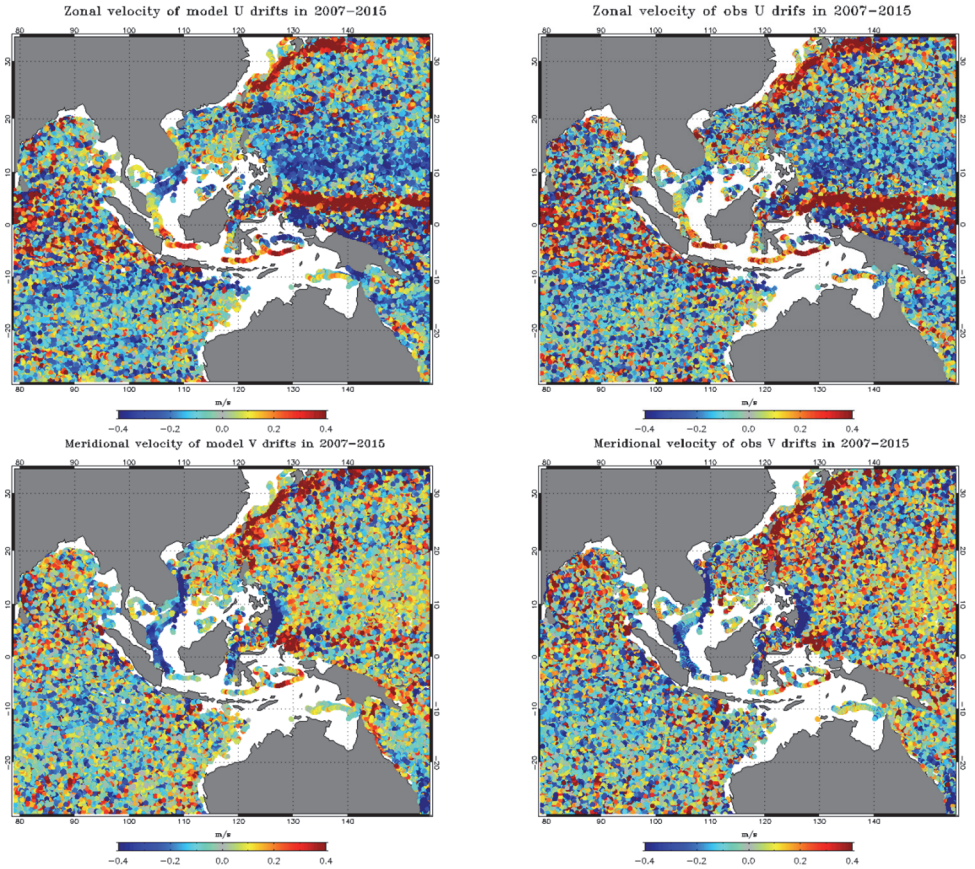


**Figure 20.21.** System 15 m current (left panels) and observation near surface drifts (right panels) from Argo surface floats and a Surface Velocity Program-corrected dataset (Rio, 2012). The zonal (top panels) and meridional (bottom panels) velocity information is indicated by a colored dot. Velocity information is averaged over the time period 2007-2015

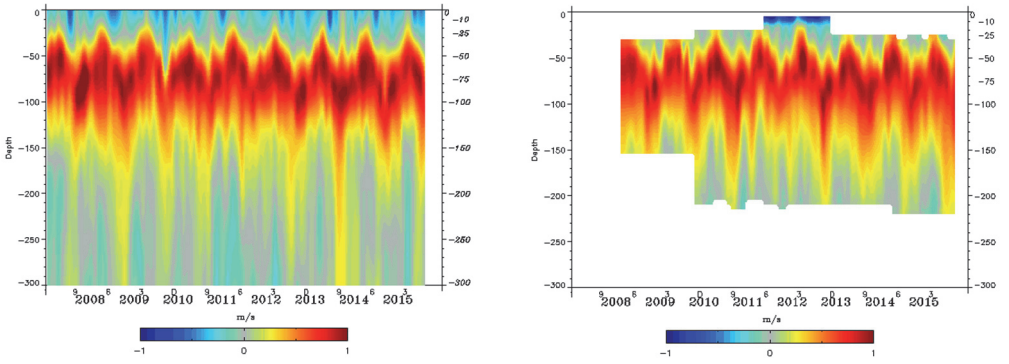


**Figure 20.22.** Vertical profiles of zonal velocity in the equatorial Atlantic at 0°N-23°W: system (on the left) and mooring data (on the right). Note that the strong westward data near the surface is questionable.

### Mooring validation

Next, we compare the Equatorial Undercurrent in the Atlantic at 0°N-23°W, as seen by the system and the PIRATA (Prediction and Research Moored Array in the Atlantic) mooring. Even if this velocity data was not assimilated into the system, the phase and intensity of the undercurrent are well-reproduced. The only concern is the core, which seems slightly too strong (Fig. 20.22).

### ALBOREX multi-platform experiment

This multi-platform experiment was conducted from 25 to 31 May 2014. The week-long experiment was designed with the objective of sampling the intense front where Atlantic and Mediterranean waters meet in the Eastern Alboran Sea and capture the intense, but transient, vertical motion associated with mesoscale and sub-mesoscale features such as ocean eddies, filaments, and fronts. Toward this goal, 24 drifters, two gliders, and three Argo floats were deployed. Drifters from the ALBOREX campaign are used here to assess the current system and the previous one. Fig. 20.23 shows SSH and velocity field for previous and current systems. Magenta dots correspond to ALBOREX drifters' positions from May 25-31 2014.

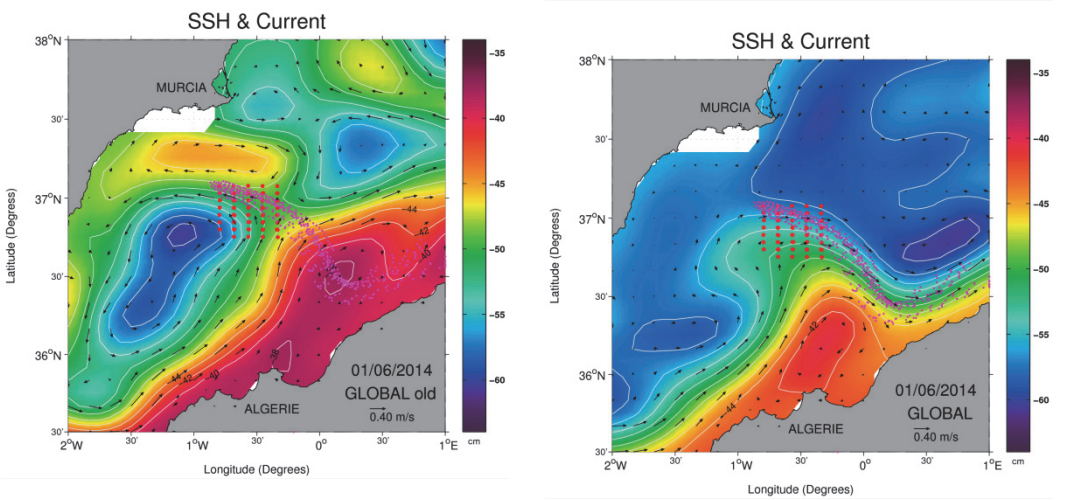


**Figure 20.23.** SSH and velocity field for previous (on the left) and current (on the right) systems. Magenta dots correspond to ALBOREX drifters' positions from May 25-31, 2014.

The previous system forecasts the intense signal of the Algerian Current flowing to the east. However, it doesn't reproduce the anticyclonic eddy and its associated front sampled during the field ALBOREX experiment. The current system significantly improves the local circulation. SSH and velocity field are in very good agreement with observations, in terms of position of the frontal zone. This improvement in the representation of the eddy and frontal zone can be attributed to the new MDT and the better-adapted prescribed SLA observation error in this region.

### Position of the Air France AF447 wreckage

On the evening of June 1, 2009, a Rio-Paris Air France flight (AF447) disappeared in a highly variable and poorly observed part of the western tropical Atlantic Ocean. The first debris from the aircraft was found five days after the accident. Several reverse drift computations were conducted

in order to define the likely position of the wreckage. Tailored high-resolution atmosphere reanalysis at Météo France and several ocean reanalyses at Mercator Ocean were produced but failed to locate the wreckage (Drévillon et al., 2013). So, in order to measure the impact of the current system updates, a new reverse drift computation was produced. Fig. 20.24 illustrates these reverse drifts using the best reanalysis from a previous Mercator system (left panel) and the current system (right panel). Circles (respectively squares) represent the model (respectively the observations) positions; the color indicates the day. The position of the wreckage is very close to the last known position (per the aircraft communications addressing and reporting system or ACARS, indicated by a black or white dot). PolSar indicates pollution observed by SAR. The best reanalysis from the previous Mercator system gave a position too far north with an estimated uncertainty of 32 km, while the new system (shown at right) locates the crash with an estimated uncertainty of only 17 km.

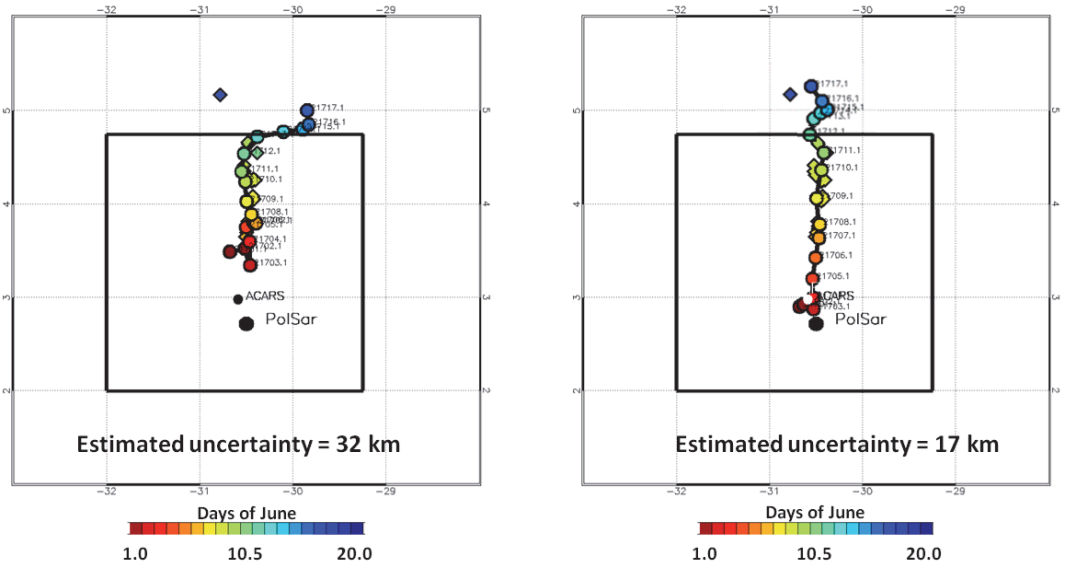


**Figure 20.24.** Illustration of reverse drifts using the best reanalysis from a previous Mercator system (left panel) and the current system (right panel). Circles (respectively squares) represent the model (respectively the observations) positions; the color indicates the day of June. The position of the wreckage is very close to the last known position (aircraft communications addressing and reporting system or ACARS, black or white dot). PolSar indicates pollution observed by SAR.

## Daily forecast validation

The performance of the daily ten-day forecasts has been checked. Fig. 20.25 represents temperature RMS differences (model minus observation) for best analysis and for one-day, three-day, five-day, seven-day, and nine-day forecasts. As expected, the best analysis has the lower RMS and this RMS increases with the forecast length. Similar results are obtained for salinity, SLA, and SST.

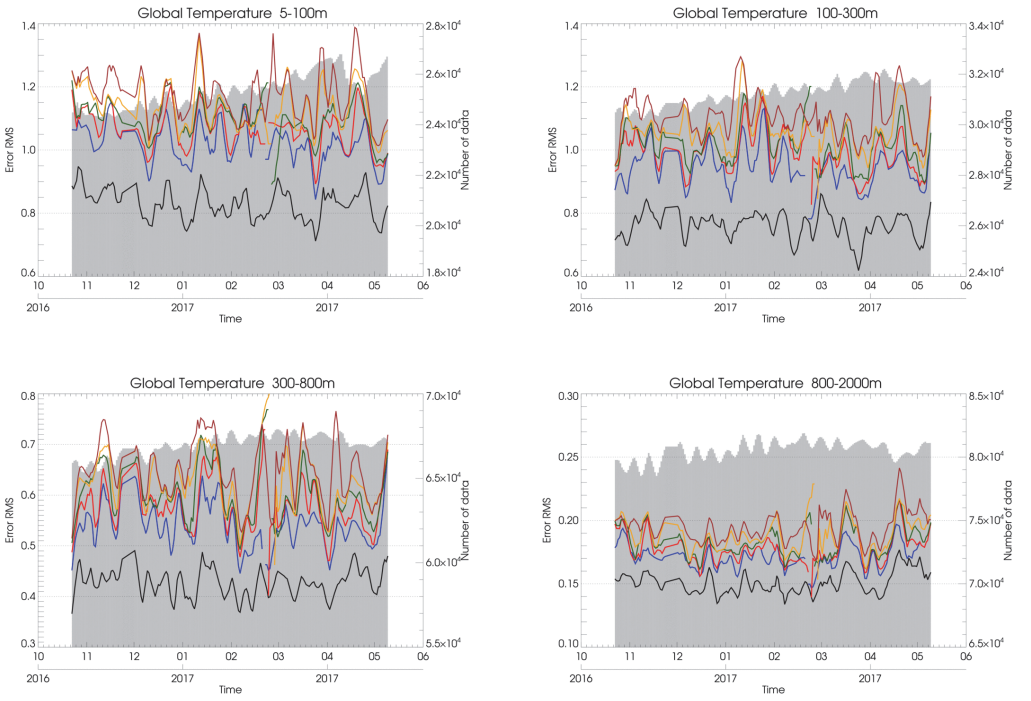


**Figure 20.25.** Global temperature (°C) RMS differences (model minus observation) in the 5-100 m, 100-300 m, 300-800 m and 800-2000 m layers. Statistics are displayed for best analysis (black line) and for one-day (blue line), three-day (red line), five-day (green), seven-day (orange line), and nine-day (brown line) forecasts. The number of available observations appears in grey in the background.

## Users and Developments

In the coming decades, strong growth of the ocean economy is expected particularly in marine aquaculture, renewable marine energies, and port activities. Scientific and technological advances will play a crucial role in addressing many of the environmental challenges of oceans and in the development of ocean-related economic activities. The ability of operational oceanography to provide relevant responses to current or future applications remains highly dependent on research and development and supply improvements. Several thematic research and development projects have been recently defined at Mercator Ocean. These projects are associated with major scientific challenges and aim to better meet the needs of users and the different applications for products delivered in real and delayed time. Products must meet the specific needs of the applications classified in the four CMEMS themes: maritime safety; marine resources management; coastal and marine environment; and weather, climate and seasonal forecasting.

The main challenges for the design of the post-2020 global Mercator Ocean system corresponds to evolutions in progress:

- Four-dimensional and ensemble-based methods to improve the analysis and provide forecast uncertainty.

- Higher 1/36° resolution consistent with high-resolution future observations (SWOT mission).
- Interaction and retroaction between ocean, waves, and atmosphere, as well as improvement of the surface layer, high-frequency phenomena including tides.
- Data assimilation of satellite sea surface salinity, ocean color, and bio-ARGO observations.

## Conclusion

The current global Mercator high-resolution system has a quite good statistical behavior with an accurate representation of the water masses, the surface fields and the mesoscale activity. Most of the components of the system have been improved compared to the previous system: global mass balance, three-dimensional T/S, sea level, sea-ice, and currents. Major variables, such as sea level and surface temperature, are hard to distinguish from the data. A 1992-to-present reanalysis is ongoing using this system, with seasonal errors for in situ vertical profiles. Future updates will deal with the assimilation of satellite sea surface salinity and the development of a four-dimensional analysis in the assimilation scheme. The remaining issues are being addressed within national and international scientific collaborations (Météo France, CNRS, CNES, ESA).

## Acknowledgments

This study has been conducted using E.U. CMEMS information. The figure related to drifters from the ALBOREX campaign was carried out as part of the CMEMS MedSUB project (PI: Simon Ruiz, CSIC). We would like to thank Hanna Kauko, Jean-Baptiste, and Christina Eunjin Kong for their participation in the summer school, as well as for their review of the manuscript and for their remarks.

## References

Amante C. and Eakins, B. W., 2009: ETOPO1 1 Arc-minute global relief model: procedures, data sources and analysis, *NOAA Technical Memorandum NESDIS NGDC-24*, 25 pp.

Arakawa, A. and Lamb, V. R., 1981: A potential enstrophy and energy conserving scheme for the shallow water equations, *Mon. Weather. Rev.*, 109, 18–36.

Barnier, B., Madec, G., Penduff, T., Molines, J. M., Treguier, A. M., Le Sommer, J., Beckmann, A., Biastoch, A., Böning, C., Dengg, J., Derval, C., Durand, E., Gulev, S., Remy, E., Talandier, C., Theetten, S., Maltrud, M., McClean, J., and De Cuevas, B., 2006: Impact of partial steps and momentum advection schemes in a global circulation model at eddy permitting resolution, *Ocean Dynam.*, 56, 543-567.

Becker, J. J., Sandwell, D. T., Smith, W. H. F., Braud, J., Binder, B., Depner, J., Fabre, D., Factor, J., Ingalls, S., Kim, S.H., Ladner, R., Marks, K., Nelson, S., Pharaoh, A., Trimmer, R., Von Rosenberg, J., Wallace, G., and Weatherall, P., 2009: Global Bathymetry and Elevation Data at 30 Arc Seconds Resolution: SRTM30_PLUS, *Mar. Geod.*, 32, 355-371, doi: 10.1080/01490410903297766.

Blanke, B. and Delecluse, P., 1993: Variability of the tropical Atlantic-Ocean simulated by a general-circulation model with 2 different mixed-layer physics, *J. Phys. Oceanogr.*, 23, 1363-1388.

Cabanes, C., Grouazel, A., Von Schuckmann, K., Hamon, M., Turpin, V., Coatanoan, C., Paris, F., Guinehut, S., Boone, C., Ferry, N., de Boyer Montégut, C., Carval, T., Reverdin, G., Pouliquen, S., and Le Traon, P.-Y., 2013: The CORA dataset: validation and diagnostics of in-situ ocean temperature and salinity measurements, *Ocean Sci.*, 9, 1-18, https://doi.org/10.5194/os-9-1-2013.

Carrère, L. and Lyard, F., 2003: Modelling the barotropic response of the global ocean to atmospheric wind and pressure forcing - comparisons with observations, *Geophys. Res. Let.*, 30(6), pp 1275.

Chambers, D.P., A. Cazenave, N. Champollion, H. Dieng, W. Llovel, R. Forsberg, K. von Schuckmann, and Y. Wada, 2017: Evaluation of the global mean sea level budget between 1993 and 2014, *Surv. Geophys.*, 38, no. 1, 309-327, doi:10.1007/s10712-016-9381-3.

Chen, J. L., Wilson, C. R., Tapley, B. D., Famiglietti, J. S., and Rodell, M., 2005: Seasonal global mean sea level change from satellite altimeter, GRACE, and geophysical models, *J. Geodesy*, 79, 532-539, doi:10.1007/s00190-005-0005-9.

Cravatte, S., Madec, G., Izumo, T., Menkes, C., and Bozec, A., 2007: Progress in the 3-D circulation of the eastern equatorial Pacific in a climate, *Ocean Model.*, 17, 28-48.

Dai A., Qian, T., Trenberth, K., and Milliman, J.D., 2009: Changes in Continental Freshwater Discharge from 1948 to 2004, *J. Climate*, vol. 22, 2773-2792.

Desroziers, G., Berre, L., Chapnik, B., and Polli, P., 2005: Diagnosis of observation, background and analysis-error statistics in observation space, *Q. J. R. Meteorol. Soc.*, 131, pp. 3385–3396, doi: 10.1256/qj.05.108.

Dibarboure, G., M.I. Pujol, F. Briol , P. Y. Le Traon , G. Larnicol , N. Picot , F. Mertz , M. Ablain, 2011: Jason-2 in DUACS: Updated System Description, First Tandem Results and Impact on Processing and Products, *Marine Geodesy*, Vol. 34, 214-241.

Drévillon, M., Greiner, E., Paradis, D., Payan, C., Lellouche, J.M., Reffray, G., Durand, E., Law-Chune, S., and Cailleau, S., 2013: A strategy for producing refined currents in the Equatorial Atlantic in the context of the search of the AF447 wreckage, *Ocean Dynamics*, 63, 63-82, DOI 10.1007/s10236-012-0580-2.

Fichefet, T. and Maqueda, M. A., 1997: Sensitivity of a global sea ice model to the treatment of ice thermodynamics and dynamics, *J. Geophys. Res.*, 102, 12609-12646.

Grasso, L. D., 2000: The differentiation between grid spacing and resolution and their application to numerical modelling, *B. Am. Meteor. Soc.*, 81, 579-580.

Grodsky, S. A., Lumpkin, R., and Carton, J. A., 2011: Spurious trends in global surface drifter currents, *Geophys. Res. Lett.*, 38, L10606, doi: 10.1029/2011GL047393.

Koch-Larrouy, A., Madec, G., Blanke, B. and Molcard, R., 2008: Water mass transformation along the Indonesian throughflow in an OGCM, *Ocean Dynam.*, 58, 289-309, doi: 10.1007/s10236-008-0155-4.

Large, W. G. and Yeager, S. G., 2009: The global climatology of an interannually varying air–sea flux data set, *Clim. Dynam.*, 33, 341-364, doi:10.1007/s00382-008-0441-3.

Lebedev, K.V., Yoshinari, H., Maximenko, N.A. and Hacker, P.W., 2007: YoMaHa'07: Velocity data assessed from trajectories of Argo floats at parking level and at the sea surface, *IPRC Technical Note*, No. 4(2)..

Lellouche, J.-M., Le Galloudec, O., Drévillon, M., Régnier, C., Greiner, E., Garric, G., Ferry, N., Desportes, C., Testut, C.-E., Bricaud, C., Bourdallé-Badie, R., Tranchant, B., Benkiran, M., Drillet, Y., Daudin, A., and De Nicola, C., 2013: Evaluation of global monitoring and forecasting systems at Mercator Océan, *Ocean Sci.*, 9, 57-81, doi:10.5194/os-9-57-2013.

Lévy, M., Estublier, A., and Madec, G., 2001: Choice of an advection scheme for biogeochemical models, *Geophys. Res. Lett.*, 28, 3725–3728, doi: 10.1029/2001GL012947.

Madec, G. and Imbard M., 1996: A global ocean mesh to overcome the North Pole singularity, *Clim. Dynam.*, 12, 381-388.

Madec, G. and the NEMO team, 2008: NEMO ocean engine. *Note du Pôle de modélisation, Institut Pierre-Simon Laplace (IPSL), France*, No. 27 ISSN, 1288-1619.

Rio, M.H., 2012: Use of altimeter and wind data to detect the anomalous loss of SVP-type drifter's drogue, *Journal of Atmospheric and Oceanic Technology*, DOI:10.1175/JTECH-D-12-00008.1.

Rio, M.-H., Mulet, S. and Picot, N., 2014: Beyond GOCE for the ocean circulation estimate: Synergetic use of altimetry, gravimetry, and in situ data provides new insight into geostrophic and Ekman currents, *Geophys. Res. Lett.*, 41, doi: 10.1002/2014GL061773.

Roquet, F., Charrassin, J. B., Marchand, S., Boehme, L., Fedak, M., Reverdin, G., and Guinet, C., 2011: Delayed-mode calibration of hydrographic data obtained from animal-borne satellite relay data loggers, *J. Atmos. Ocean. Tech.*, 28, 787–801.

Roullet, G., and Madec, G., 2000: Salt conservation, free surface, and varying levels: a new formulation for ocean general circulation models, *J. Geophys. Res.*, 105, 23927–23942.

Silva, T. A. M., Bigg, G. R., and Nicholls, K. W., 2006: Contribution of giant icebergs to the Southern Ocean freshwater flux, *J. Geophys. Res.*, 111, C03004, doi: 10.1029/2004JC002843.

Tranchant, B., Reffray, G., Greiner, E., Nugroho, D., Koch-Larrouy, A., and Gaspar, P., 2016: Evaluation of an operational ocean model configuration at 1/12° spatial resolution for the Indonesian seas (NEMO2.3/INDO12) – Part 1: Ocean physics, *Geosci. Model Dev.*, 9, 1037-1064.